New structure induced by elastic anisotropy in cylindrical nematic liquid crystal

Zhang Qian, Zhou Xuan, Zhang Zhidong*
Department of Physics, Hebei University of Technology, Tianjin 300401, China;
*E-Mail: zhidong_zhang1961@163.com

ABSTRACT

Basing on Landau–de Gennes theory, this study investigated the chiral configurations of nematic liquid crystals confined to cylindrical capillaries with homeotropic anchoring on the cylinder walls. When the elastic anisotropy (L_2/L_1) is large enough, a new structure results from the convergence of two opposite escape directions of the heterochiral twist and escape radial (TER) configurations. The new defect presents when $L_2/L_1 \geq 7$ and disappears when $L_2/L_1 < 7$. The new structure possesses a heterochiral hyperbolic defect at the center and two homochiral radial defects on both sides. The two radial defects show different chiralities.

Keywords

Landau-de Gennes theory; escape radial configurations; elastic anisotropy; defect

Academic Discipline And Sub-Disciplines

Physics, Liquid Crystal Physics

SUBJECT CLASSIFICATION

Condensed matter

TYPE (METHOD/APPROACH)

Theoretical

1 INTRODUCTION

The equilibrium configuration of a confined nematic liquid crystal (NLC) introduces a rich phenomenology of defects. Among widely used geometries, nematics in cylindrical capillaries exhibit a particularly rich diversity of structures that primarily depend on molecular orientation at the walls of the confining capillaries [1]. The structures in cylindrical cavities with homeotropic anchoring have three possible types: (a) planar polar (PP), (b) planar radial (PR), and (c) escaped radial (ER) [2–4]. Many experiments [5–10] show that in cylinders with radii R=0.5–200μm, ER configuration is realized, while in cylinders with radii R=0.05– 0.4μm, either ER or PP configuration can occur, and in cylinders with radii R≤0.1μm, PR can occur [4, 6, 8, 11–12]. There are two 1/2 line defects in PP configuration, and a +1 line defect in PR configuration. In ER configuration, the two degenerate escape directions that lead to two possible types of defects are radial defect and hyperbolic defect [13–15].

The elastic properties of nematic liquid crystals (LCs) are crucial for LC display applications [16, 17], and they continue to give rise to unanticipated fundamental phenomena [18–28]. Recent studies have found that cylinders with broken chiral symmetry exhibit a lyotropic chromonic LC (LCLC), which has a small twist elastic constant (K22) [29–31]. A twist and escape radial (TER) configuration was found in cylindrical cavities with homeotropic anchoring. The chirality of the configurations can be either right or left handed. The two different escape directions with opposite senses of handedness in the configuration also lead to two possible types of defects: radial and hyperbolic. Moreover, the defects with the same handedness are unstable [19].

In this study, we investigated a new structure resulting from the convergence of two opposite escape directions of heterochiral TER configurations with a large-enough elastic anisotropy. Our study is based on Landau–de Gennes theory and a 2D finite-difference iterative method. The outline of the paper is as follows. In section 2, we introduce the phenomenological model employed and describe the geometry of the problem and our parameterization. The results are presented in Section 3, and the conclusions are summarized in Section 4.

2 MODELING

2.1 Free energy

Our theoretical argument is based on Landau–de Gennes theory [32], wherein the orientational order of LC is described by a second-rank symmetric and traceless tensor [33]:

$$Q = \sum_{i=1}^{3} \lambda_i \vec{e}_i \otimes \vec{e}_i, \tag{1}$$

where $\vec{e}_i$, for i=1, 2, 3, are the orthogonal unit vectors representing the eigenvectors of Q, and λ_i are the corresponding eigenvalues. Q vanishes in the isotropic phase, possessing two degenerate eigenvalues in the uniaxial ordering and can be represented by

$$Q = S\left(\vec{n} \otimes \vec{n} - \frac{1}{3}\mathrm{I}\right), \tag{2}$$

where $\vec{n}$ is the nematic director pointing along the local uniaxial ordering direction, and S is the uniaxial scalar parameter expressing the nematic director's fluctuation magnitude.

The LC is in a biaxial state when all eigenvalues of Q are distinct. The degree of biaxiality is expressed by the parameter β^2 defined as [34]

$$\beta^2 = 1 - \frac{6\left[tr\left(Q^3\right)\right]^2}{\left[tr\left(Q^2\right)\right]^3}. \tag{3}$$

This equation presents a convenient parameter for illustrating spatial inhomogeneities of Q and ranges in the interval [0, 1]. All uniaxial states with two degenerate eigenvalues correspond to $\beta^2 = 0$, whereas states with maximal biaxiality correspond to $\beta^2 = 1$. As $tr(Q^3)$=3det$Q$, states with $\beta^2 = 1$ are those with det$Q$=0, implying that at least one eigenvalue of Q vanishes.

The Landau–de Gennes free energy density of NLC is given by $f = f_{\text{bulk}} + f_{\text{elastic}}$,where

$$f_{\text{bulk}} = \frac{A}{2} trQ^2 - \frac{B}{3} trQ^3 + \frac{C}{4}\left(trQ^2\right)^2, \tag{4}$$

is the bulk energy that describes a homogeneous phase. In Eq. (4), B and C are positive constants, and A is assumed to vary with temperature T in the form of $A = A_0 (T - T^*)$, where A_0 is a positive constant and T^* is the nematic supercooling temperature. Eq. (4) provides the bulk equilibrium value of the uniaxial scalar order parameter in Eq. (2) $S_{\text{eq}}=B\left(1+\left(1-24AC/B^2\right)^{1/2}\right)\Big/4C$, which depends on the temperature.

The free-energy felastic, which penalizes gradients in the tensor order parameter field, is given in the form [35, 36]

$$f_{\text{elastic}} = \frac{1}{2}L_1\left(\nabla Q \vdots \nabla Q\right) + \frac{1}{2}L_2\left(\nabla \cdot Q\right)\cdot\left(\nabla \cdot Q\right) + \frac{1}{2}L_3 Q : \left(\nabla Q : \nabla Q\right), \tag{5}$$

where L_1, L_2 and L_3 are elastic constants. Corresponding to Frank theory, we obtain the relationship between L_i and K_{ii} [36],

$$\begin{aligned} L_1 &= \frac{3K_{22} - K_{11} + K_{33}}{6S^2}, \\ L_2 &= \frac{K_{11} - K_{22}}{S^2}, \\ L_3 &= \frac{K_{33} - K_{11}}{2S^2}. \end{aligned} \tag{6}$$

Here, we assume $K_{11} = K_{33} \neq K_{22}$, that is,

$$\begin{aligned} L_1 &= \frac{K_{22}}{2S^2}, \\ L_2 &= \frac{K_{11} - K_{22}}{S^2}, \\ L_3 &= 0. \end{aligned} \tag{7}$$

In Eqs. (6) and (7), K_{11}, K_{22} and K_{33} are splay, twist and bend elastic constants in Frank theory, respectively. It means that the system has elastic anisotropy, and the free-energy felastic can be rewritten as

$$f_{\text{elastic}} = \frac{1}{2}L_1\left(\nabla Q \,\vdots\, \nabla Q\right) + \frac{1}{2}L_2\left(\nabla \cdot Q\right)\cdot\left(\nabla \cdot Q\right). \tag{8}$$

2.2 Geometry of the problem

Let us consider an NLC confined in capillaries with homeotropic boundary conditions. The LC directors are radial near the capillary wall and bend along the radius to be parallel to the cylindrical axis of the capillary; two degenerate directions of bend deformations are found, and the choice between the two deformations determines the escape direction. In essence, the system can minimize elastic free energy by producing a TER configuration when it has a small twist elastic constant K_{22} [19].

To describe the configuration, standard polar cylindrical coordinates (ρ,ϕ,z) and the corresponding local frame $(\vec{e}_\rho,\vec{e}_\phi,\vec{e}_z)$ are introduced, as shown in Figure 1a, where $\vec{e}_z$ points along the symmetry axis, $\vec{e}_\rho$ is the radial unit vector emanating from the symmetry axis, and $\vec{e}_\phi := \vec{e}_z \times \vec{e}_\rho$. In the polar cylindrical coordinates, the nematic director is given by $\vec{n} = \sin\gamma\cos\alpha\vec{e}_\rho + \sin\gamma\sin\alpha\vec{e}_\phi + \cos\gamma\vec{e}_z$, where the polar angle γ is the angle between the z unit vector ($\vec{e}_z$) and the director $\vec{n}$, and the twist angle α is the angle between the ρ unit vector ($\vec{e}_\rho$) and the $\rho-\phi$ projection ($n_{\rho\phi}$) of the director. In the cylindrical coordinate system, Eq. (2) can be written in matrix form as

$$Q = \begin{pmatrix} Q_{\rho\rho} & Q_{\rho\phi} & Q_{\rho z} \\ Q_{\phi\rho} & Q_{\phi\phi} & Q_{\phi z} \\ Q_{z\rho} & Q_{z\phi} & Q_{zz} \end{pmatrix} = S\begin{pmatrix} n_\rho n_\rho - \frac{1}{3} & n_\rho n_\phi & n_\rho n_z \\ n_\rho n_\phi & n_\phi n_\phi - \frac{1}{3} & n_\phi n_z \\ n_\rho n_z & n_\phi n_z & n_z n_z - \frac{1}{3} \end{pmatrix}. \tag{9}$$

LC molecules are strongly anchored along the perpendicular directions of the cylinder walls. To research it advantageously, the LC texture is assumed to exhibit a cylindrical symmetry along the cylindrical axis, i.e., the nematic orientation is independent of ϕ. Accordingly, the texture can be discussed in terms of 2D nematics corresponding to each radial slice.

We denote the free boundary conditions at the upper and lower lateral walls. The new configuration requires $\gamma(\rho=0)=0$ at the center with free boundary conditions, as well as homeotropic strong anchoring on the cylinder walls given by $\gamma(\rho=R)=\pm\pi/2$ and $\alpha(\rho=R)=0$, which correspond to the −z or z escape direction, respectively. In our simulation, the initial value is given as follows: From the center of the cylinder to the wall, the polar angle changes from 0 to $\pm\pi/2$, and the twist angle changes linearly from $\pi/2$ to 0. Figures 1(b)–1(d) show the initial profile of the director. Figures 1(c) and 1(d) are the perspective views of about the bottom half and the top half in Figure 1(b), representing left-handed and right-handed chiralities, respectively.

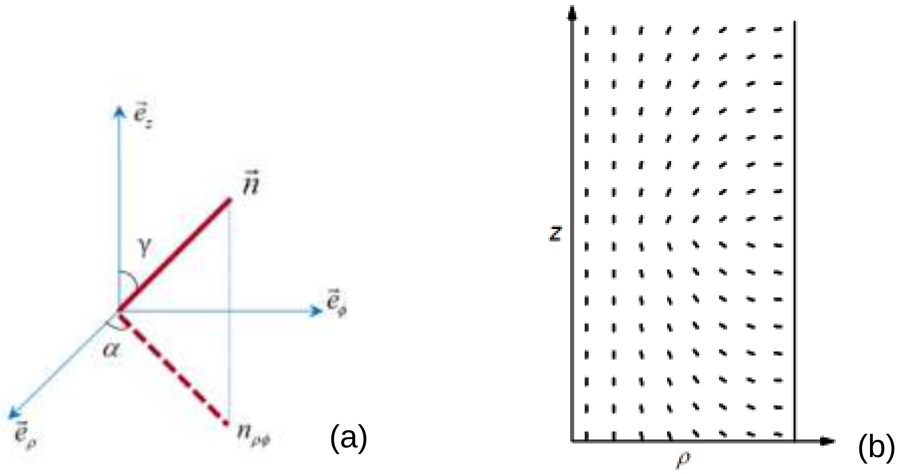

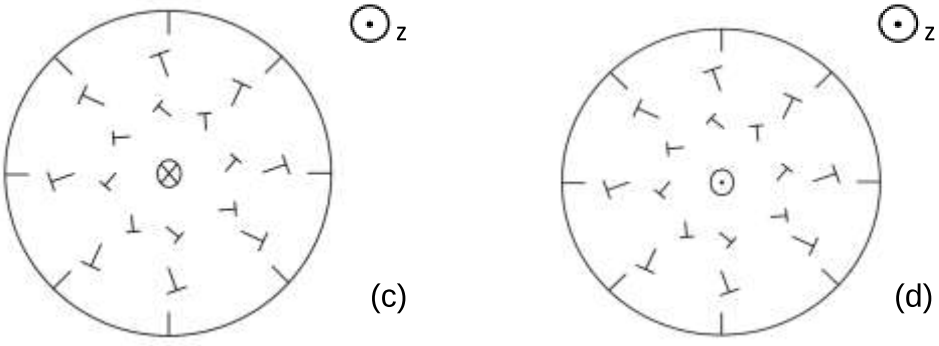

(c) (d)

Fig 1: Geometry of the problem. (a) Cylindrical coordinate system (ρ, ϕ, z) used to describe the configuration. (b) Director profile in a cross-section along an arbitrary radius of the system. (c) and (d) provide the cross-sectional view of (b).

2.3 Scaling and dimensionless evolution equations

We introduce the following dimensionless quantities: $\tilde{f} \equiv f \Big/ \dfrac{B^4}{64C^3}$, $\tilde{z} \equiv z/\xi_0$, $\tilde{\rho} \equiv \rho/\xi_0$, $\tilde{Q}_{ij} \equiv Q_{ij}/q_0$, where $q_0 := S_{eq}\left(T^{**}\right) = B/4C$ is the superheating order parameter at the nematic superheating temperature T**, and $\xi_0 := \sqrt{L_1/Bq_0} = \sqrt{4CL_1/B^2}$ is the characteristic length for order-parameter changes. Given that Q is symmetric and traceless, that is $Q_{\rho\phi}=Q_{\phi\rho}$, $Q_{\rho z}=Q_{z\rho}$, $Q_{\phi z}=Q_{z\phi}$, $Q_{\rho\rho}+Q_{\phi\phi}+Q_{zz}=0$, we leave five independent variables only, thus Eqs. (4) and (8) can be expressed by

$$\begin{aligned}
\tilde{f}_{bulk} = {} & \frac{\tilde{A}}{12}\left(2\tilde{Q}_{\rho\rho}^{\ 2} + 2\tilde{Q}_{\phi\phi}^{\ 2} + 2\tilde{Q}_{\rho\phi}^{\ 2} + 2\tilde{Q}_{\rho z}^{\ 2} + 2\tilde{Q}_{\phi z}^{\ 2} + 2\tilde{Q}_{\rho\rho}\tilde{Q}_{\phi\phi}\right) \\
& -\frac{1}{3}\Big\{\tilde{Q}_{\rho\rho}\left(\tilde{Q}_{\rho\rho}^{\ 2} + \tilde{Q}_{\rho\phi}^{\ 2} + \tilde{Q}_{\rho z}^{\ 2}\right) + \tilde{Q}_{\phi\phi}\left(\tilde{Q}_{\rho\phi}^{\ 2} + \tilde{Q}_{\phi\phi}^{\ 2} + \tilde{Q}_{\phi z}^{\ 2}\right) \\
& -\left(\tilde{Q}_{\rho\rho} + \tilde{Q}_{\phi\phi}\right)\left(\tilde{Q}_{\rho z}^{\ 2} + \tilde{Q}_{\phi z}^{\ 2} + \tilde{Q}_{\rho\rho}^{\ 2} + \tilde{Q}_{\phi\phi}^{\ 2} + 2\tilde{Q}_{\rho\rho}\tilde{Q}_{\phi\phi}\right) \\
& + 2\tilde{Q}_{\rho\phi}\left(\tilde{Q}_{\rho\rho}\tilde{Q}_{\phi\phi} + \tilde{Q}_{\rho\phi}\tilde{Q}_{\phi\phi} + \tilde{Q}_{\rho z}\tilde{Q}_{\phi z}\right) + 2\tilde{Q}_{\rho z}\left(\tilde{Q}_{\rho\rho}\tilde{Q}_{\rho z} + \tilde{Q}_{\rho\phi}\tilde{Q}_{\phi z} - \tilde{Q}_{\rho\rho}\tilde{Q}_{\rho z} - \tilde{Q}_{\rho z}\tilde{Q}_{\phi\phi}\right) \\
& + 2\tilde{Q}_{\phi z}\left(\tilde{Q}_{\rho\phi}\tilde{Q}_{\rho z} + \tilde{Q}_{\phi\phi}\tilde{Q}_{\phi z} - \tilde{Q}_{\rho\rho}\tilde{Q}_{\phi z} - \tilde{Q}_{\phi z}\tilde{Q}_{\phi\phi}\right)\Big\} \\
& + \frac{1}{16}\left(2\tilde{Q}_{\rho\rho}^{\ 2} + 2\tilde{Q}_{\phi\phi}^{\ 2} + 2\tilde{Q}_{\rho\rho}\tilde{Q}_{\phi\phi} + 2\tilde{Q}_{\rho\phi}^{\ 2} + 2\tilde{Q}_{\rho z}^{\ 2} + 2\tilde{Q}_{\phi z}^{\ 2}\right)^2,
\end{aligned} \tag{10}$$

$$\begin{aligned}\tilde{f}_{elastic} = \frac{1}{2}\Bigg\{ & 2\left(\frac{\partial \tilde{Q}_{\rho\rho}}{\partial \tilde{\rho}}\right)^2 + 2\left(\frac{\partial \tilde{Q}_{\rho\rho}}{\partial \tilde{z}}\right)^2 + 2\left(\frac{\partial \tilde{Q}_{\phi\phi}}{\partial \tilde{\rho}}\right)^2 + 2\left(\frac{\partial \tilde{Q}_{\phi\phi}}{\partial \tilde{z}}\right)^2 + 2\frac{\partial \tilde{Q}_{\rho\rho}}{\partial \tilde{\rho}}\frac{\partial \tilde{Q}_{\phi\phi}}{\partial \tilde{\rho}} + 2\frac{\partial \tilde{Q}_{\rho\rho}}{\partial \tilde{z}}\frac{\partial \tilde{Q}_{\phi\phi}}{\partial \tilde{z}} \\ & + 2\left[\left(\frac{\partial \tilde{Q}_{\rho z}}{\partial \tilde{\rho}}\right)^2 + \left(\frac{\partial \tilde{Q}_{\rho z}}{\partial \tilde{z}}\right)^2\right] + 2\left[\left(\frac{\partial \tilde{Q}_{\rho\phi}}{\partial \tilde{\rho}}\right)^2 + \left(\frac{\partial \tilde{Q}_{\rho\phi}}{\partial \tilde{z}}\right)^2\right] + 2\left[\left(\frac{\partial \tilde{Q}_{\phi z}}{\partial \tilde{\rho}}\right)^2 + \left(\frac{\partial \tilde{Q}_{\phi z}}{\partial \tilde{z}}\right)^2\right] \\ & + \frac{2}{\tilde{\rho}^2}\left(\tilde{Q}_{\rho\rho}^{\,2} + \tilde{Q}_{\phi\phi}^{\,2} + 4\tilde{Q}_{\rho\phi}^{\,2} + \tilde{Q}_{\phi z}^{\,2} + \tilde{Q}_{\rho z}^{\,2} - 2\tilde{Q}_{\rho\rho}\tilde{Q}_{\phi\phi}\right)\Bigg\} \qquad (11) \\ & + \frac{1}{2}\frac{L_2}{L_1}\Bigg\{\left(\frac{\partial}{\partial \tilde{\rho}}\tilde{Q}_{\rho\rho} + \frac{\partial}{\partial \tilde{z}}\tilde{Q}_{z\rho} + \frac{\tilde{Q}_{\rho\rho} - \tilde{Q}_{\phi\phi}}{\tilde{\rho}}\right)^2 + \left(\frac{\partial}{\partial \tilde{\rho}}\tilde{Q}_{\rho\phi} + \frac{\partial}{\partial \tilde{z}}\tilde{Q}_{z\phi} + \frac{2\tilde{Q}_{\rho\phi}}{\tilde{\rho}}\right)^2 \\ & + \left(\frac{\partial}{\partial \tilde{\rho}}\tilde{Q}_{\rho z} - \frac{\partial}{\partial \tilde{z}}\left(\tilde{Q}_{\rho\rho} + \tilde{Q}_{\phi\phi}\right) + \frac{\tilde{Q}_{z\rho}}{\tilde{\rho}}\right)^2\Bigg\}.\end{aligned}$$

where the reduced parameter $\tilde{A} = 24AC/B^2$ defines the temperature scale. Isotropic–nematic transition occurs at $\tilde{A} = 8/9$. The values of L_2/L_1 represent the magnitude of the elastic anisotropy. Eq. (6) shows that a larger value of L_2/L_1 corresponds to a smaller twist elastic constant K_{22}.

We compute the evolution of LC with dynamic theory for tensor order-parameter field Q (ρ, z, t). The local values of the scalar-order parameter S and the director $\vec{n}$ can be calculated from Q by using the highest eigenvalue and the associated eigenvector, respectively. According to [37], the evolution equation describing the dynamics of Q can be written as

$$\frac{\partial Q}{\partial t} = \Gamma\left(-\frac{\delta f}{\delta Q}\right), \qquad (12)$$

where $\Gamma = 6D^*/[1-3\mathrm{tr}(Q^2)]^2$, D^* is the rotational diffusion for the nematic.

Numerical calculations are performed using the reduced variables. When the functional derivatives in Eq. (12) are evaluated and the derivatives are discretized with a finite difference, the partial differential equations for $\tilde{Q}$ can be obtained as follows:

$$\left[\tilde{Q}(t+\Delta t) - \tilde{Q}(t)\right] / \Delta t = -\tilde{\Gamma}\frac{\delta \tilde{f}}{\delta \tilde{Q}}, \qquad (13)$$

where

$$\frac{\delta \tilde{f}}{\delta \tilde{Q}} = \frac{\partial \tilde{f}}{\partial \tilde{Q}_{ij}} - \frac{\partial}{\partial \tilde{\rho}}\frac{\partial \tilde{f}}{\partial \tilde{Q}_{ij,\tilde{\rho}}} - \frac{1}{\tilde{\rho}}\frac{\partial \tilde{f}}{\partial \tilde{Q}_{ij,\tilde{\rho}}} - \frac{\partial}{\partial \tilde{z}}\frac{\partial \tilde{f}}{\partial \tilde{Q}_{ij,\tilde{z}}} \qquad (14)$$

with $\tilde{\Gamma} = \Gamma \times (Bq_0)$. We adopt the 2D finite-difference method developed in our previous studies [38, 39] to obtain the numerical simulation results. Here, we let the system relax from the initial boundary conditions given in Section 2.2. In our numerical calculations, we adopted a proper time step to guarantee the stability of the numerical procedure. In addition, our equilibration runs were verified to be adequate for the system to reach equilibrium.

3. RESULTS AND DISCUSSION

In this section, we present our numerical results. According to the parameters given in [40], $A_0 = 0.195 \times 10^6$ J/m^3, B = 7.155×10^6 J/m^3, C = 8.82×10^6 J/m^3, and $L_1 = 10.125 \times 10^{-12}$ J/m can be easily obtained. In our simulations, the scaled temperature is set to $\tilde{A} = 2/3$, which corresponds to $\tilde{S} = 1 + \sqrt{1/3}$. The rotational diffusion D^* is set to 0.35, which is the value used in [40]. The exact value of ξ_0 is 2.64 nm. In order to get rich defect structures, a small radius R is choosen in our simulation. We set H=600ξ_0 and R=150ξ_0, where H and R represent the lengths along the z- and ρ-axes, respectively. More precise in calculation, the *z*-axis is discretized into 242 small intervals with $\Delta z = b\xi_0\left(b = 2.5\right)$, and the *ρ*-axis is discretized into 121 small intervals with $\Delta\rho = a\xi_0\left(a = 1.25\right)$.

3.1. Discovery of the new structure

We simulate the defect structures which were found to arise in experiment when the two opposite escape directions of the heterochiral TER configuration diverge and converge with L_2/L_1=18. As expected, It is shown that a hyperbolic defect and a radial defect ring appear in our simulation. Then we investigate the change of the two structures with elastic anisotropy (L_2/L_1). A radial defect is found with smaller elastic anisotropy L_2/L_1(This part will be published in else where). While when L_2/L_1 is large enough, a new structure forms. Figure. 2 gives the new structure in a cross-section along an arbitrary azimuth in detail with L_2/L_1=30.

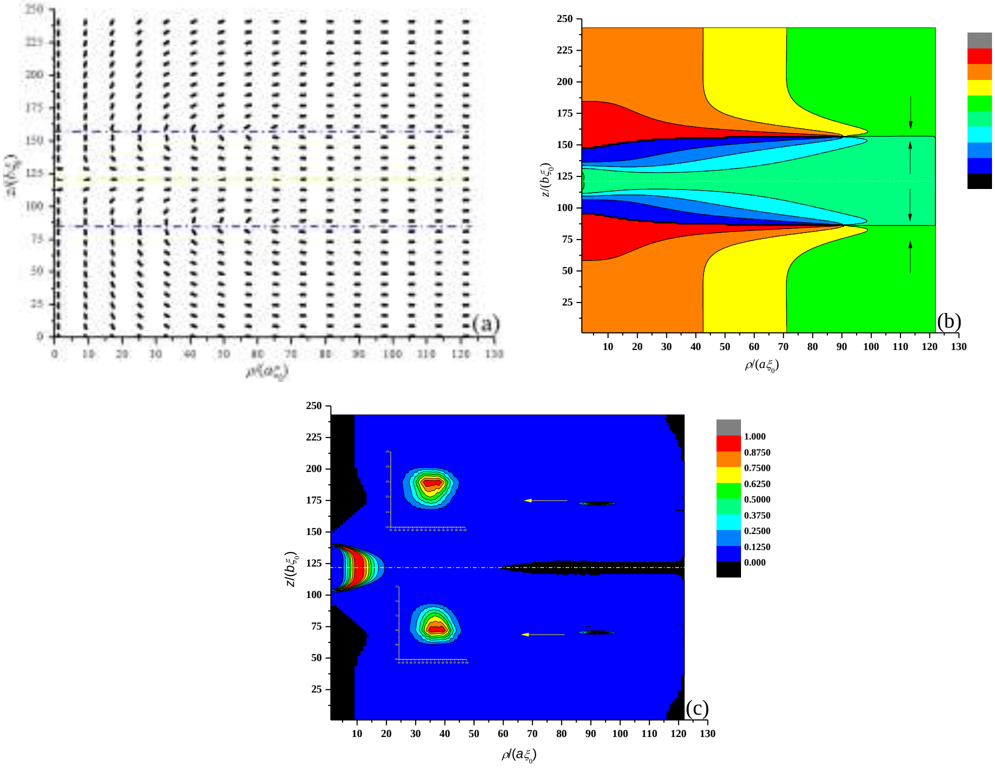

Fig 2: New structure with L_2/L_1=30. (a) Director-field, (b) Twist angle *α*, (c) Biaxiality β^2.

Figure 2(a) shows the director profile in a cross-section along an arbitrary radius of the system. We found a hyperbolic defect at the center of the system and two radial defects on both sides. The yellow dot–dash line represents the center of the hyperbolic defect, and the blue dot–dash lines represent the center of the two radial defects. In the vicinity of the center plane layer, the LC directors are radial forming a PR structure. In Figure 2(b), the black arrows indicate escape directions. Combined with the director profile, the nucleuses on both sides have different chiralities. The top half is left-handed, whereas the bottom half is right-handed. Figure 2(c) shows the biaxiality of the defect. At the center of the defect, the biaxiality has a maximum size. For the axis-symmetry of the structure, the radial defects present as biaxiality rings, and the hyperbolic defect presents as a biaxiality shell.

To sum up, three defects were found in the new structure, one heterochiral hyperbolic defect containing a planar polar structure and two homochiral radial defects. The hyperbolic defect is formed when the two homochiral radial defects coupled. The homochiral radial defects on the top and bottom halves have different chiralities. For any half of the new defect, it is shown a radial defect in our numerical simulation; however, it is unstable in the experiment [19].

3.2 Relationship between new structure and elastic anisotropy

3.2.1 Effect of elastic anisotropy on spontaneous distortion

Figure 3 shows the relationship between elastic anisotropy and spontaneous distortion by twist angle. The layered structure remains the same until approximately L_2/L_1≈7. When L_2/L_1<7, the layered structure disappears. When the elastic anisotropy L_2/L_1 is reduced, the distance between the two radial defects and the z-axis is shortens, whereas the part with *α*=0 compresses to the center plane layer.

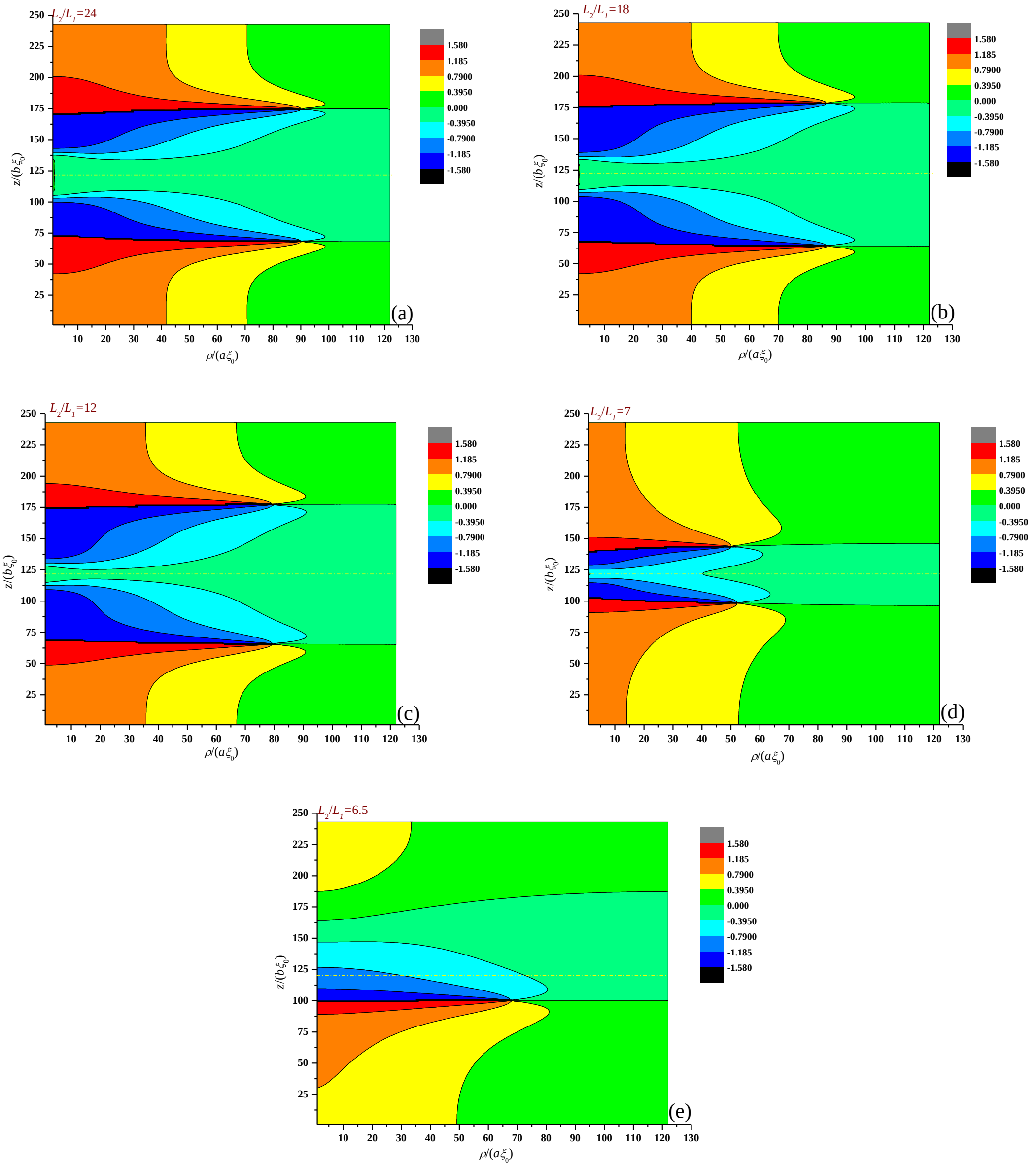

Fig 3: Variation of twist angle when L_2/L_1 is 24 (a), 18 (b), 12 (c), 7 (d), and 6.5 (e), respectively.

3.2.2 Influence of elastic anisotropy on new structure

Figures 4 and 5 show the director field profile and the calculated biaxiality β^2 in a cross-section along an arbitrary azimuth for different values of L_2/L_1. When the elastic anisotropy is reduced, the distance between two radial defects (see the blue dot–dash lines in Figure 4) initially thickens and then thins, whereas the PR structure keeps thinning. When $L_2/L_1<7$, a structure transition happens with a +1/2 defect below the central plane layer. Figure 5 shows that the two radial defects move toward the symmetry axis z and the hyperbolic defect shrinks as the elastic anisotropy is reduced. When $L_2/L_1<7$, the hyperbolic defect is annihilated by merging with the radial defect of the upper half, leaving only the lower half of the homochiral defect ring. Hence, the new defect structure can exist in systems with $L_2/L_1\geq7$.

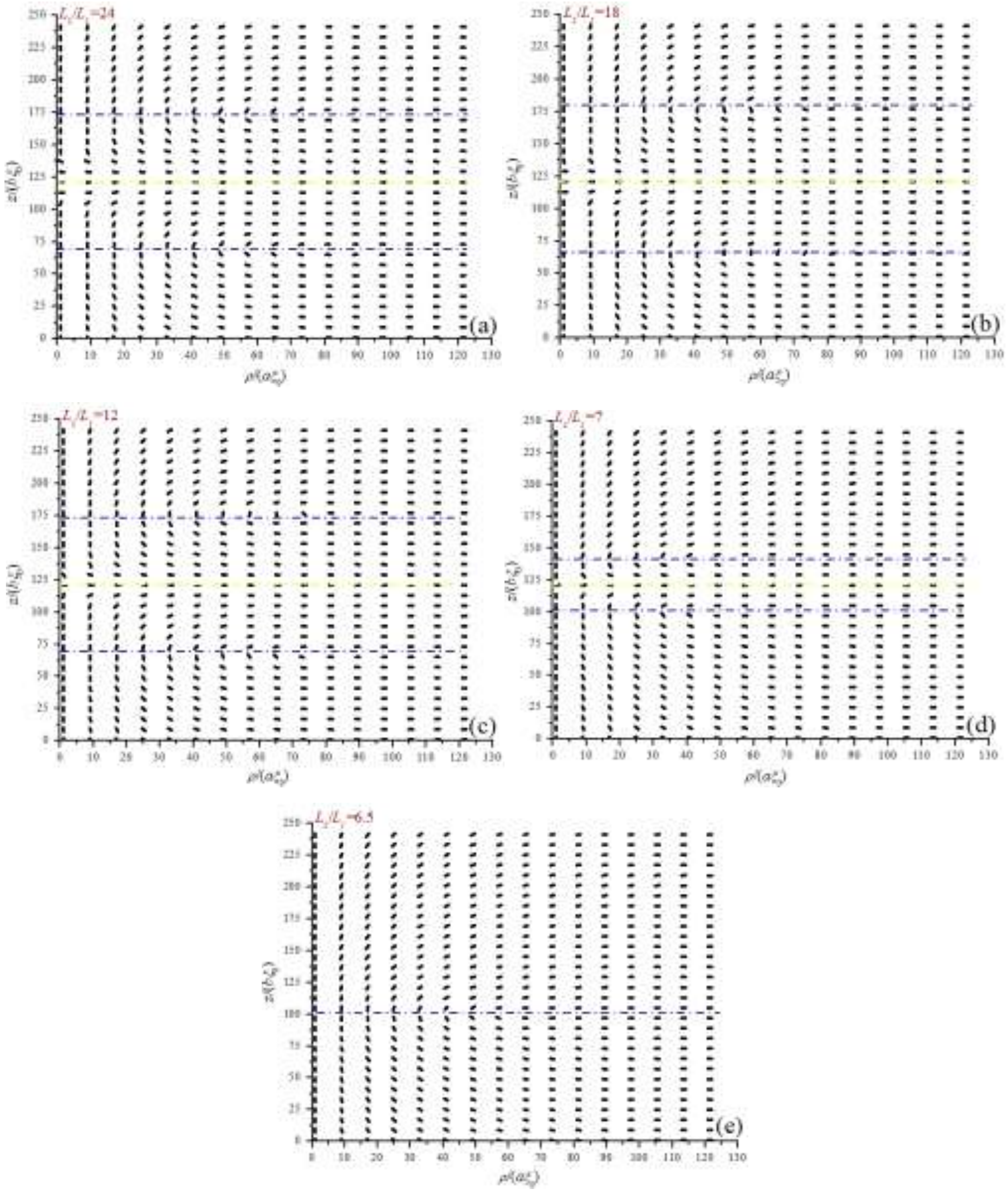

Fig 4: Variation of director fields with reducing elastic anisotropy.

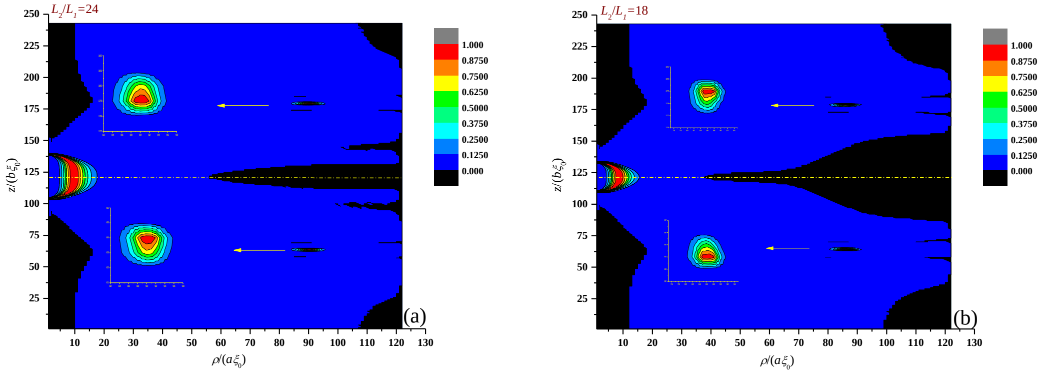

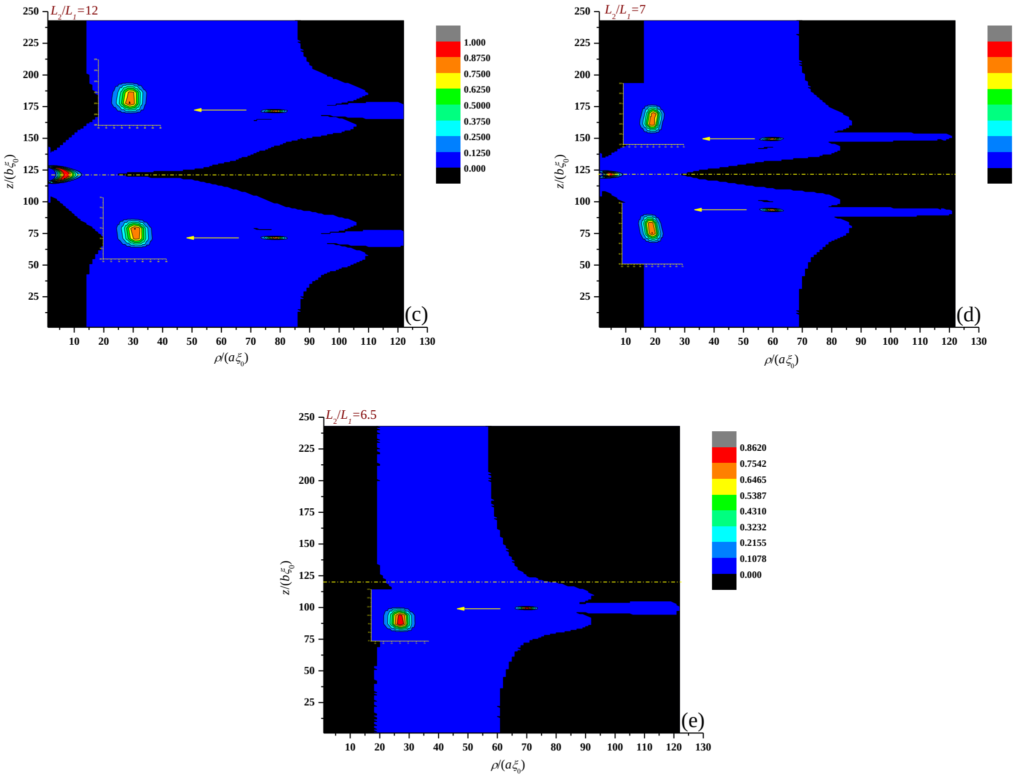

Fig 5: Variation of biaxiality β^2 with reducing elastic anisotropy.

3.3 Effect of free boundary on new structure

In our simulation, free boundary conditions are prescribed at the upper and lower lateral walls. The next discussion is the impact of the boundary conditions on new defects. The length of z is extended on both sides, and the extended length is H=1200ξ_0. Figure 6 shows the structure of the system with H=1200ξ_0 and L_2/L_1=18.

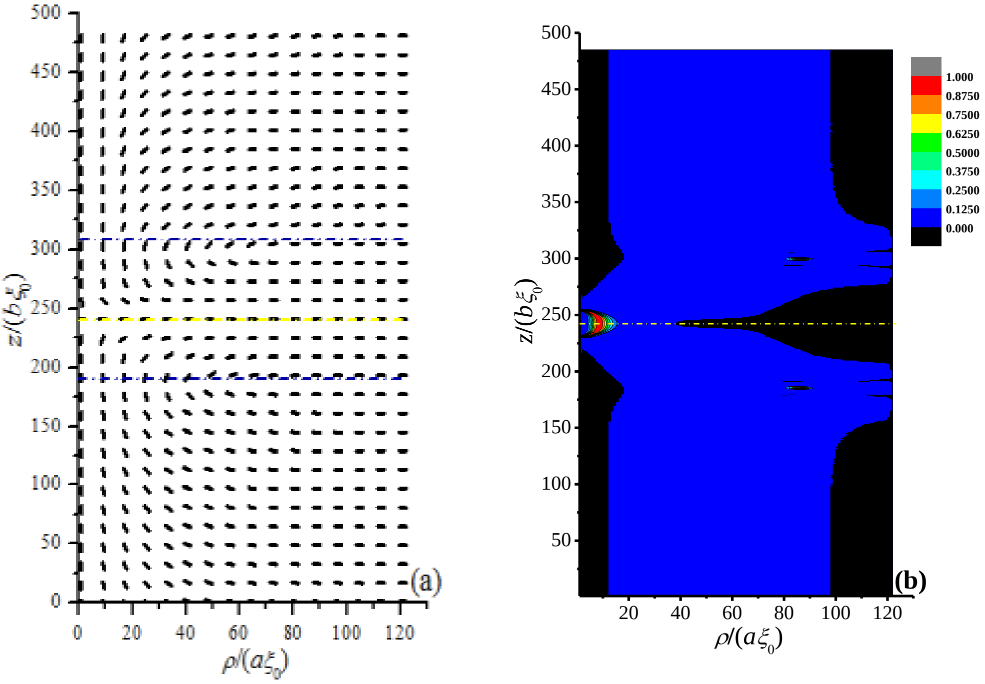

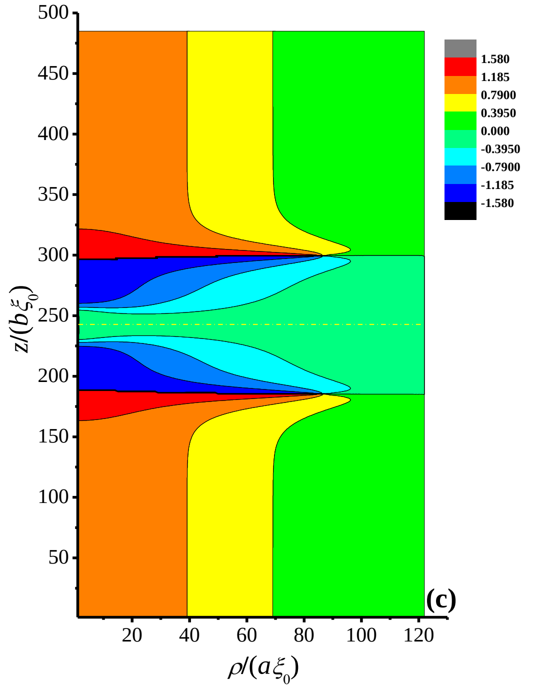

Fig 6: New structure when H=1200ξ_0. (a) Director-field, (b) Twist angle α, (c) Biaxiality β^2.

In the progress of our simulation, the z-axis is discretized into 484 small intervals, and the ρ-axis is discretized into 121 small intervals, indicating that the size of each interval remains the same. Comparison of Figures 3(b), 4(b), 5(b) and Figures 6(c), 6(a), 6(b) shows no change in the size of the blue dashed frame and the spontaneous distortion. The defect position and its shape remain almost unchanged, indicating that the free boundary exerts no influence on the basic structure.

3.4. Energy of new structure

We calculate the energy of radial defect, hyperbolic defect, TER structure, and the new defect. As shown in Figure 7, with the increase of the elastic anisotropic, the energy of four kinds of structures increases. Moreover, the energy of TER is higher than that of the hyperbolic defect and lower than that of the radial defect. The results coincide well with that given by Frank theory in [19]. And this maybe the reason why the structure of radial defect changed and created a new structure while the hyperbolic one did not. In addition, the energy of the new structure is lower than that of the radial defect when $L_2/L_1 \geq 10$ and higher than it when $L_2/L_1 < 10$; and it is higher than the energy of TER and hyperbolic structures with all values of L_2/L_1. It is given in [19] that radial defects and hyperbolic defects are metastable in the experiment, so we speculated that the new defect is also metastable, and its stability needs to be verified in experiment.

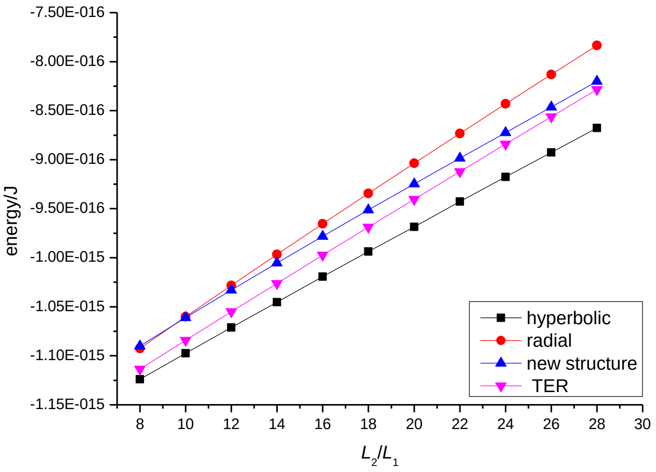

Fig 7: The energy of four configurations.

4. CONCLUSION

When the elastic anisotropy is large enough, a new structure is resulted from the convergence of two opposite escape directions of the heterochiral TER configurations. Three defects can be found in the new structure: one heterochiral hyperbolic defect containing a PR structure and two homochiral radial defects. The most interesting feature in the new structure is the hyperbolic defect that formed when the two homochiral radial defects coupled. Moreover, the homochiral radial defects on the top and bottom halves have different chiralities. In fact, each side of the new defect is unstable in the experiment. The new defect disappears when $L_2/L_1<7$. The effects of spontaneous distortion and boundary conditions were also studied. Spontaneous distortion is a prerequisite for the stability of new defects, whereas free boundary exerts no effect on it.

In our Landau theory, $L_2/L_1=7$ corresponds to $K_{11}:K_{22}:K_{33}=1:0.22:1$ in frank elastic theory. This larger elastic anisotropy is difficult for the thermotropic LC to achieve, which is more researched in capillary experiment than the LCLC. The stability of the new structure needs to be further explored in future experiments, with our work providing theoretical guidance for experiment.

ACKNOWLEDGMENTS

This research was supported by the National Natural Science Foundation of China under Grant No. 11374087 and the Key Subject Construction Project of Hebei Province University

REFERENCES

1. Svetec, M.,and Slavinec, M. 2008.Structural transition of nematic liquid crystal in cylindrical capillary as a result of the annihilation of two point defects. J. Chem. Phys. 128 (8), 4117.
2. Crawford, G. P., Ondris-Crawford, R. J.,Doane, J. W.,and Zumer, S. 1996. Systematic study of orientational wetting and anchoring at a liquid-crystal-surfactant interface. Phys. Rev. E 53(4), 3647-3661.
3. Shams, A., Yao, X., Park, J. O., Srinivasarao, M.,and Rey, A. D. 2014. Theoretical predictions of disclination loop growth for nematic liquid crystals under capillary confinement. Phy. Rev. E 90(4-1), 042501.
4. Burylov, S. V. 1997. Equilibrium configuration of a nematic liquid crystal confined to a cylindrical cavity. J. Exp. Theor. Phys. 85(5), 873-886.
5. Allender, D. W., Crawford, G. P., and Doane, J. W. 1991.Determination of the liquid-crystal surface elastic constant K24. Phys. Rev. Lett. 67(11), 1442-1445.
6. Crawford, G. P., Allender, D. W., and Doane, J. W. 1992. Surface elastic and molecular-anchoring properties of nematic liquid crystals confined to cylindrical cavities. Phys. Rev. A 45(12), 8693-8708.
7. Crawford, G. P., Vilfan, M., Doane, J. W., and Vilfan, I. I. 1991. Escaped-radial nematic configuration in submicrometer-size cylindrical cavities: Deuterium nuclear-magnetic-resonance study. Phys. Rev. A 43(2), 835-842.
8. Ondris-Crawford, R. J., Crawford, G. P., Doane, J. W., ŽUmer, S.; Vilfan, M., and Vilfan, I. I. 1993. Surface molecular anchoring in microconfined liquid crystals near the nematic–smectic-A transition. Phys. Rev. E 48(3), 1998-2005.
9. Crawford, G. P., Allender, D. W., Doane, J. W., Vilfan M., and Vilfan, I. I. 1991. Finite molecular anchoring in the escaped-radial nematic configuration: A NMR 2 study. Phys Rev A 44, 2570-2577.
10. Scharkowski, A., Crawford, G. P., . ŽUmer, S., and Doane, J. W. 1993. A method for the determination of the elastic constant ratio K33/K11 in nematic liquid crystals. J. App. Phys. 73(11), 7280-7287.
11. Meyer, R. B. 1973. On the existence of even indexed disclinations in nematic liquid crystals. [J]. Philos. Mag. 27(2), 405-424.
12. Cladis, P. E., and Kléman, M. 1972 Non-singular disclinations of strength S= + 1 in nematics. J. Phys. 33(5-6), 591-598.
13. Lavrentovich, O. D. 2003. Defects in Liquid Crystals: Surface and Interfacial Anchoring Effects. Springer Netherlands, Patterns of Symmetry Breaking.
14. De, L. G., and Rey, A. D. 2007.Point and ring defects in nematics under capillary confinement. J. Chem. Phys. 127(10), 2013-2018.
15. Kralj, S., and ŽUmer, S. 1995. Saddle-splay elasticity of nematic structures confined to a cylindrical capillary. Phys. Rev. E 51(1), 366-379.
16. Schadt, M., and Helfrich, W. 1971. Voltage- dependent optical activity of a twisted nematic liquid crystal.Appl. Phys. Lett. 18(4), 127-128.
17. Yeh, P., and Gu, C. 2010.Optics of Liquid Crystal Displays (Wiley, Hoboken, New Jersey, 2010).

18. Jeong, J., Davidson, Z. S., Collings, P. J., Lubensky, T. C., and Yodh, A. G. 2014. Chiral symmetry breaking and surface faceting in chromonic liquid crystal droplets with giant elastic anisotropy. Proc. Natl. Acad. Sci. 111(5), 1742-1747.
19. Jeong, J., Kang, L., Davidson, Z. S., Collings, P. J., Lubensky, T. C., and Yodh, A. G. 2015. Chiral structures from achiral liquid crystals in cylindrical capillaries. Proc. Nat. Acad. Sci. 112(15), 1837-1844.
20. Škarabot, M., Ravnik, M., Žumer, S., Tkalec, U., Poberaj, I., Babič, D., and Muševič, I. 2008. Hierarchical self-assembly of nematic colloidal superstructures. Phys. Rev. E 77(6), 061706.
21. Rao, L., Ge, Z., Wu, S. T., and Lee, S. H. 2009. Low voltage blue-phase liquid crystal displays. Appl. Phys. Lett. 95(23), 231101.
22. Gibaud, T., Barry, E., Zakhary, M. J., Henglin, M., Ward, A., Yang, Y., Berciu, C., Oldenbourg, R., Hagan, M. F., Nicastro, D., Meyer, R. B., and Dogic, Z. 2012. Reconfigurable self-assembly through chiral control of interfacial tension. Nature 481(7381), 348-351.
23. Jones, C. 2012. in Handbook of Visual Display Technology, edited by Chen, J., Cranton, W., and Fihn, M. (Springer, Berlin,) pp. 1507-1543.
24. Li, Q. 2012. Liquid Crystals Beyond Displays: Chemistry, Physics, and Applications. John Wiley & Sons.
25. James, R., and Fukuda, J. 2014. Twist transition of nematic hyperbolic hedgehogs. Phys. Rev. E 89(4), 749-773.
26. Williams, R. D. 1986. Two transitions in tangentially anchored nematic droplets. J. Phys. A-Math. Gen. 19(16), 3211-3222.
27. Lavrentovich, O. D., and Sergan, V. V. 1990. Parity-breaking phase transition in tangentially anchored nematic drops. II Nuovo Cimento D 12(9), 1219-1222.
28. Lavrentovich, O. D., and Terentjev, E. M. 1986. Phase transition altering the symmetry of topological point defects (hedgehogs) in a nematic liquid crystal Sov. Phys. JETP 64(6): 1237-1244.
29. Davidson, Z. S., Kang, L., Jeong, J., Still, T., Collings, P. J.,. Lubensky, T.C, and Yodh, A. G. 2015. Chiral structures and defects of lyotropic chromonic liquid crystals induced by saddle-splay elasticity Phys. Rev. E 91(5), 050501.
30. Zhou, S., Nastishin, Y. A.,. Omelchenko, M. M, Tortora, L., Nazarenko, V. G., Boiko, O. P., Ostapenko, T., Hu, T., Almasan, C. C., Sprunt, S. N., Gleeson, J. T., and Lavrentovich, O. D. 2012. Elasticity of lyotropic chromonic liquid crystals probed by director reorientation in a magnetic field. Phys Rev Lett. 109(3), 514-514.
31. Zhou, S., Neupane, K., Nastishin, Y. A., Baldwin, A. R., Shiyanovskii, S. V., Lavrentovich, O. D., and Sprunt, S. 2014. Elasticity, viscosity, and orientational fluctuations of a lyotropic chromonic nematic liquid crystal disodium cromoglycate. Soft Matter 10(34), 6571-6581.
32. De Gennes, P.G., and Prost, J. 1993. The Physics of Liquid Crystals, Oxford University Press, Oxford, UK,
33. Virga, E. G. 1994. Variational theories for liquid crystals. Chap-man Hall.
34. Kaiser, P., Wiese, W., and Hess, S. 2015. Stability and Instability of an Uniaxial Alignment Against Biaxial Distortions in the Isotropic and Nematic Phases of Liquid Crystals.J. Non-Equil. Thermody. 17(2), 153-170.
35. Soulé, E. R., Abukhdeir, N. M., and Rey, A. D. 2009. Theory and computation of directional nematic phase ordering. Phys Rev E 79(1), 1-28.
36. Amoddeo, A., Barberi, R., and Lombardo, G. 2014. Electric field-induced fast nematic order dynamics. Liq Cryst, 41. 1219-1228
37. Guzmán, O., Abbott, N. L. and de Pablo, J. J. 2005. Quenched disorder in a liquid-crystal biosensor: Adsorbed nanoparticles at confining walls. J. Chem. Phys. 122(18), 1307-1326.
38. Zhou, X., and Zhang, Z. D. 2012. Dynamics of order reconstruction in a nanoconfined nematic liquid crystal with a topological defect. 14(12), 24135-53.
39. Zhou, X., and Zhang, Z. D. 2014. Dynamics of order reconstruction in nanoconfined twisted nematic cells with a topological defect. Liq. Cryst. 41(9), 1219-1228.
40. Qian, T. Z., and Sheng, P. 1997. Orientational states and phase transitions induced by microtextured substrates.Phys Rev E 55(55), 7111-7120.

Author' biography with Photo

Qian Zhang received the B.S. degree from the Department of Physics and Electronic Engineering, Baoding University, Hebei, China, in 2010. He is currently working toward the M.S. degree for liquid crystal devices at Hebei University of technology,TianJin, China.

Xuan Zhou received the M.S. degree in liquid crystal fields from Hebei University of technology, TianJin, China, in 2010, and the Ph.D. degree in condensed matter physics fields from Changchun Institute of Optics, Fine Mechanics and Physics Chinese Academy of Science, Changchun, China, in 1998.

Zhidong Zhang received the M.S. degree in theoretical physics from HeBei University of technology, TianJin, China, in 1987, and the Ph.D. degree in liquid crystal fields from Changchun Institute of Optics, Fine Mechanics and Physics Chinese Academy of Science, Changchun, China, in 1998.